Viscous second gradient porous materials for bones reconstructed with bio-resorbable grafts

Ivan Giorgio, Ugo Andreaus, Francesco Dell 'Isola, Tomasz Lekszycki

Viscous second gradient porous materials for bones reconstructed with bio-resorbable grafts

Ivan Giorgio[a,c,*], Ugo Andreaus[a], Francesco dell'Isola[a,c], Tomasz Lekszycki[b,c]

[a] *Dep. of Structural and Geotechnical Engineering, Università di Roma La Sapienza 18 Via Eudossiana, Rome, Italy*
[b] *Warsaw University of Technology, Warsaw, Poland*
[c] *International Research Center for the Mathematics and Mechanics of Complex Systems - MeMoCS, Università dell'Aquila Cisterna di Latina, Italy*

Abstract

It is well known that size effects play an important role in the mechanical behavior of bone tissues at different scales. In this paper we propose a second gradient model for accounting these effects in a visco-poro-elastic material and present some sample applications where bone is coupled with bioresorbable artificial materials of the kind used in reconstructing surgery.

Keywords: Metamaterials, second gradient materials, porous media, viscous dissipation, bone remodelling
2010 MSC: 00-01, 99-00

1. Introduction

Substantial size effects are known to occur in the elastic behavior of (i) single osteons [1], (ii) human compact bone [2, 3, 4, 5, 6], (iii) human trabecular bone [7, 8]. In the first case, the size effects are attributed to compliance of the interfaces between laminae. In the second case, there is experimental evidence that the cement lines as compliant interfaces account for most of the difference in stiffness between osteons and whole bone. In the third case, continuum properties vary by more than 20-30% over a distance spanning three to five trabeculae and hence a continuum model for the structure is suspect [7]. Therefore, Ramézani et al. [8] used the Cosserat theory to describe the hierarchical multi-scale behavior of trabecular human bone using micro-CT images, namely: i) macroscale, dealing with cancellous bone or spongy bone at real size; ii) meso-scale, representing non-homogeneous and stochastic network clusters; iii) micro-scale, indicating the micro-randomness and heterogeneous deformations; iv) sub-micro- and nano-scale, showing single lamellas including collagen fibers and apatite crystals. Generally speaking, the limitations of the continuum assumption appear in two areas: near biologic interfaces, and where there are large stress gradients. To incorporate the scale of the microstructure of a heterogeneous material within the continuum framework, a number of phenomenological 'remedies' have been proposed that involve the relaxation of the local action hypothesis of classical continuum mechanics. Such enriched (or enhanced) continuum models aim at including information on the microstructure and can be classified into three main groups [9], namely: (i) non-local integral models [10, 11], (ii) higher-order gradient models [12, 13, 14] and (iii) micropolar theories [15, 16, 17]. Bleustein [18] showed how the boundary conditions of a linear theory of an elastic continuum with micro-structure [19] can be reduced to those of a corresponding linear form of a strain gradient theory [20]. Following this way of thinking, second gradient materials can be interpreted as a particular limit case of micromorphic (or micropolar) media because they can be deduced from micromorphic ones by constraining the micromorphic kinematic descriptors to be equal to the classical strain ones by introducing internal constraints and Lagrange multipliers. We remark that this constrained approach which is rigorous in a finite-dimensional space, it is assumed reasonably acceptable in an infinite-dimensional space on the basis of an argument of analogy. This paper is inspired by the more general framework of a research oriented to design the mechanical characteristics of the biomaterial constituting the graft, namely mass density and resorption velocity, in order to optimize the mass density distribution of the growing bone tissue. The continuum model employed in this paper is accordingly richer than standard Cauchy continuum, including higher gradients of displacement in the deformation energy. The addition of terms in the energy involving second gradient of the displacement arises from the consideration of the geometry of the trabecular structure of the bone. Trabeculae are indeed organized (locally) as a lattice system oriented along

the principal stress directions [21]. Since a not negligible amount of deformation energy is stored in the form of bending of trabeculae [22], a classic Cauchy model is not sufficiently rich and instead terms in the energy describing the curvature of the microstructure have to be considered. This fact naturally leads to second gradient energy models. More generally, it has been proven [23] that high contrast at micro-level of mechanical properties can impose at macro-level the need of introducing deformation energies depending on higher displacement gradient. In general, generalized continuum theories such as couple stress and micropolar have degrees of freedom in addition to those of classical elasticity [24, 25]: however, in the case of the second gradient models this is not needed [18]. All such theories are thought to be applicable to materials with fibrous or granular structure. Experimentally Yang and Lakes measured the effect of size on apparent stiffness of compact bone in quasi-static torsion [3] and bending [4].

2. Material and methods

The considered specimen is constituted by the union of two bi-dimensional square portions, one constituted of bone tissue and the other of biomaterial; the square size is $L/2 = W = 0.5$ cm. The mass densities of the two materials are initially assigned in each zone and they will evolve in the subsequent remodeling process according to the mechanical and biological laws presented in the following (see Eq. (17)). The support conditions on one edge are shown in a self-explanatory way in Fig. 1.

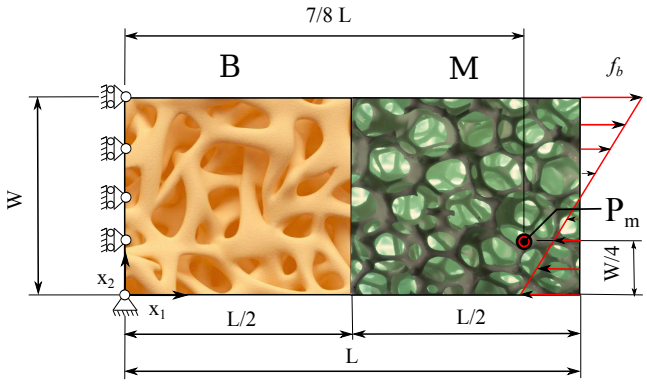

Figure 1: Sample under study at initial stage. The labels "B" and "M" stand for bone and graft material, respectively.

A traction distribution corresponding to a pure bending is applied to the opposite edge as shown in Fig. 1; the load is harmonically variable with a low frequency Ω in order to activate the component of the stimulus which is related to dissipation, because this phenomenon plays a key role in the bone functional adaptation, as discussed in [26]. In particular, we set

$$f_b(x_2, t) = \left(\frac{2x_2}{W} - 1\right)[F_0 + F_1 \sin(\Omega t)] \qquad (1)$$

Some relevant results will be presented with reference to the probe point P_m in the material zone (Fig. 1).

3. Governing Equations

Kinematics. In order to give a macroscopic description of the system under study constituted by an insert of bioresorbable grafting material and a piece of bone, i.e. a porous mixture, we introduce the placement field:

$$\boldsymbol{\chi} : (\boldsymbol{X}, t) \mapsto \boldsymbol{x} \qquad (2)$$

which takes each point of body $\boldsymbol{X}$ in the reference configuration $\mathcal{B}$ and time $t \in \mathbb{R}$ into a place $\boldsymbol{x}$ in the current configuration. Therefore, we consider the solid-matrix macroscopic displacement ($\boldsymbol{u} = \boldsymbol{x} - \boldsymbol{X}$) as a basic kinematical descriptor and use the Saint-Venant strain tensor

$$E_{\mathrm{ij}}(\mathbf{X}, t) = \frac{1}{2}\left(u_{\mathrm{i,j}} + u_{\mathrm{j,i}} + u_{\mathrm{i,k}}\, u_{\mathrm{k,j}}\right) \qquad (3)$$

to take elastic deformations into account. Because of the porous nature of our system, we introduce another independent kinematical descriptor to describe the microdeformations of pores inside the solid matrix of the system. In particular, we introduce the change of the Lagrangian porosity, i.e. the change of the effective volume of the fluid content per unit volume of the body with respect to an equilibrium volume [27]. In detail,

$$\zeta(\mathbf{X}, t) = \phi(\boldsymbol{\chi}(\mathbf{X}, t), t) - \phi^*(\mathbf{X}, t) \qquad (4)$$

where ϕ and ϕ^* are the Lagrangian porosity related to the current and the reference configuration, respectively. By adopting the approach of the mixture theory, these porosities can be expressed as follows

$$\phi = 1 - (\rho_{\mathrm{b}}/\hat{\rho}_{\mathrm{b}} + \rho_{\mathrm{m}}/\hat{\rho}_{\mathrm{m}}), \quad \phi^* = 1 - (\rho^*_{\mathrm{b}}/\hat{\rho}_{\mathrm{b}} + \rho^*_{\mathrm{m}}/\hat{\rho}_{\mathrm{m}}) \qquad (5)$$

where ρ_{b} and ρ_{m} are the apparent mass densities of bone tissue and artificial material, respectively; the superimposed hat denotes the true densities, while the superscript * indicates all quantities in the reference configuration.

Variational equation of motion. As already mentioned, the bone is organized at micro-level as a three-dimensional porous network of interconnected trabeculae (cancellous bone). It can be also seen as a quasi-periodic system of cylindroid structures, i.e. osteons, (cortical bone) characterized by a high contrast of mechanical properties between bending and extension. Therefore, using the classical framework of Poromechanics (Biot [27], Cowin [28]) and second gradient continua (Mindlin [19], Toupin [20]), for the potential energy-density —potential energy per

unit of macro-volume— we take a homogeneous, quadratic function of the variables $\boldsymbol{E}$, $\nabla\boldsymbol{E}$, ζ and $\nabla\zeta$ [29, 30, 13]

$$\begin{aligned}\mathscr{E} = &\frac{1}{2}\lambda(\rho_{\rm b}^*,\rho_{\rm m}^*)\,E_{\rm ii}E_{\rm jj} + \mu(\rho_{\rm b}^*,\rho_{\rm m}^*)\,E_{\rm ij}E_{\rm ij} + \\ &4\,\alpha_1(\rho_{\rm b}^*,\rho_{\rm m}^*)E_{\rm ii,j}E_{\rm jk,k} + \alpha_2(\rho_{\rm b}^*,\rho_{\rm m}^*)E_{\rm ii,j}E_{\rm kk,j} + \\ &4\,\alpha_3(\rho_{\rm b}^*,\rho_{\rm m}^*)E_{\rm ij,i}E_{\rm kj,k} + 2\,\alpha_4(\rho_{\rm b}^*,\rho_{\rm m}^*)E_{\rm ij,k}E_{\rm ij,k} + \\ &4\,\alpha_5(\rho_{\rm b}^*,\rho_{\rm m}^*)E_{\rm ij,k}E_{\rm ik,j} + \frac{1}{2}K_1(\rho_{\rm b}^*,\rho_{\rm m}^*)\zeta^2 + \\ &\frac{1}{2}K_2\zeta_{,\rm i}\zeta_{,\rm i} - K_3(\rho_{\rm b}^*,\rho_{\rm m}^*)\,\zeta\,E_{\rm ii} \end{aligned} \tag{6}$$

where λ and μ are the Lamé parameters

$$\lambda = \frac{\nu\,Y(\rho_{\rm b}^*,\rho_{\rm m}^*)}{(1+\nu)(1-2\nu)}, \qquad \mu = \frac{Y(\rho_{\rm b}^*,\rho_{\rm m}^*)}{2(1+\nu)}, \tag{7}$$

here expressed in terms of the Young modulus of the mixture

$$Y = Y_{\rm b}^{\rm Max}(\rho_{\rm b}^*/\hat{\rho}_{\rm b})^2 + Y_{\rm m}^{\rm Max}(\rho_{\rm m}^*/\hat{\rho}_{\rm m})^2 \tag{8}$$

and Poisson ratio. $Y_{\rm b}^{\rm Max}$ and $Y_{\rm m}^{\rm Max}$ are the maximal elastic moduli. The second gradient stiffness coefficients are assumed to be:

$$\begin{aligned}&\alpha_1 = \alpha_2 = \alpha_4 = Y(\rho_{\rm b}^*,\rho_{\rm m}^*)\ell^2,\ \alpha_3 = 2Y(\rho_{\rm b}^*,\rho_{\rm m}^*)\ell^2,\\ &\alpha_5 = 1/2Y(\rho_{\rm b}^*,\rho_{\rm m}^*)\ell^2\end{aligned} \tag{9}$$

being ℓ a suitable scale length of the microstructure, i.e., in this case, it is related to the diameter of trabeculae or osteons which are around 200 μm. The coefficient K_1 is a coefficient of compressibility related to the bone marrow inside pores and can be evaluated as

$$K_1 = \left(\frac{\phi^*}{K_{\rm f}} + \frac{(\alpha_B-\phi^*)(1-\alpha_B)}{K_{\rm dr}}\right)^{-1} \tag{10}$$

depending on the stiffness of marrow $K_{\rm f}$ and the drained bulk modulus of the porous matrix $K_{\rm dr} = Y/(3(1-2\nu))$, α_B being the Biot-Willis coefficient. K_2, assumed to be constant, is a parameter which takes into account the gradient of porosity, i.e., a non-local stiffness related to interaction phenomena among neighboring pores. The coupling between microstructure and solid bulk is assumed to be

$$K_3 = \sqrt{\hat{g}(\phi^*)\,\lambda\,K_1} \tag{11}$$

where the weight

$$\hat{g}(\phi^*) = \frac{0.9}{\pi}\left\{\operatorname{atan}\left[15\left(\phi^*-\frac{1}{2}\right)\right] + \operatorname{atan}\left(\frac{15}{2}\right)\right\} \tag{12}$$

is a monotonically increasing function which modulates the micro-macro coupling depending on the reference porosity.

To model dissipative phenomena, we employ a Rayleigh dissipation function

$$2\mathcal{D}_s = 2\mu^v\left(\dot{E}_{\rm ij}\dot{E}_{\rm ij} - \frac{1}{3}\dot{E}_{\rm ii}\dot{E}_{\rm jj}\right) + \kappa^v\,\dot{E}_{\rm ii}\dot{E}_{\rm jj} \tag{13}$$

related to the solid-matrix macroscopic rate strain. The material parameters κ^v and μ^v are the bulk and shear viscosity coefficients, respectively.

The Generalized Principle of Virtual Work, including dissipation effects and neglecting inertia terms, for independent variations $\delta u_{\rm i}$ and $\delta\zeta$, therefore, runs as follows

$$-\int_{\mathcal{B}}\delta\mathscr{E}\,{\rm d}\,\mathcal{B} + \int_{\mathcal{B}}\delta\mathscr{W}^{\rm ext}{\rm d}\,\mathcal{B} = \int_{\mathcal{B}}\frac{\partial\mathcal{D}_s}{\partial\dot{E}_{\rm ij}}\delta E_{\rm ij}{\rm d}\,\mathcal{B} \tag{14}$$

where $\delta\mathscr{W}^{\rm ext}$ is the variation of the work done by external actions. The assumed potential energy-density (6) is the motivation for the adoption of the following form for the variation of work done by external action:

$$\delta\mathscr{W}^{\rm ext} = \int_{\partial_\tau\mathcal{B}}\tau_{\rm i}\delta u_{\rm i}{\rm d}\mathcal{S} + \int_{\partial_\tau\mathcal{B}}T_\alpha\delta u_{\alpha,\rm j}n_{\rm j}{\rm d}\mathcal{S} + \int_{\partial\mathcal{B}}\Xi\,\delta\zeta{\rm d}\mathcal{S}, \tag{15}$$

where body and line forces are neglected, $\tau_{\rm i}$ is the surface traction on the boundary, and T_α is an external double force per unit of area, i.e., a mechanical 'dipole action' [31] which consists in two opposite forces, with zero resultant, acting on two points which can be considered distinct only at the length scale of the micro-structure, i.e. trabeculae or osteons (see for more details on physical interpretation [19, 32]) and resulting in a macro-deformation exclusively in a higher gradient continuum (while such an external action is irrelevant in a simple Cauchy theory), Ξ is a micro-structural action which describes the local dilatant behavior of a porous material induced by pore opening, capillary interaction phenomena among neighboring pores.

It is worth noting that a second gradient continuum model can be deduced via an homogenization procedure based on micro-macro identification to obtain an equivalent model which reproduces at the macro scale the behavior of the material characterized by a complex microstructure at micro-scale (see e.g. [33, 14, 34]). In this homogenization process, some critical issues as for instance a damage occurring in the bone tissue or in the biomaterial can be taken into account (see e.g. [35, 36, 37]).

Interface modeling. Interface conditions can be formulated by adding to the energy density (6) an internal boundary extra term:

$$\mathscr{E}_{\rm int} = \frac{1}{2}K_\zeta\,[\![\zeta]\!]^2 + \frac{1}{2}K_u\,[\![\boldsymbol{u}]\!]\cdot[\![\boldsymbol{u}]\!] + \frac{1}{2}K_{\nabla u}\,[\![(\nabla\boldsymbol{u})\boldsymbol{n}]\!]\cdot[\![(\nabla\boldsymbol{u})\boldsymbol{n}]\!] \tag{16}$$

This simple interface potential energy-density can be useful to better describe the real conditions of connection between bone tissue and artificial material with a proper choice of the stiffnesses characterizing the mechanical properties of the junction layer, K_ζ, K_u and $K_{\nabla u}$, which, respectively, define an elastic interaction due to the jump in the fields of ζ, $\boldsymbol{u}$ and $\nabla\boldsymbol{u}$ for the two different regions jointed. The symbol $[\![\cdot]\!]$ stands for the jump of any field $f(\boldsymbol{X})$ through the interface, i.e., $[\![f]\!] = f^+ - f^-$).

Evolution rules. The evolution of the apparent mass densities is governed by the rules [38, 39]:

$$\begin{cases} \dot{\rho}^*_{\mathrm{b}} = A_{\mathrm{b}}\,(S)\; H\,(\phi) & \text{with } 0 < \rho^*_{\mathrm{b}} \leqslant \hat{\rho}_{\mathrm{b}} \\ \dot{\rho}^*_{\mathrm{m}} = A_{\mathrm{m}}\,(S)\; H\,(\phi) & \text{with } 0 < \rho^*_{\mathrm{m}} \leqslant \rho^*_{\mathrm{m}}(\boldsymbol{X}, 0) \end{cases} \tag{17}$$

which are assumed to depend on the mechanical stimulus S resulting from an external applied load and the current porosity ϕ. The functions A_{b} and A_{m} are taken to be

$$A_{\{\mathrm{b,m}\}}\,(S) = \begin{cases} s_{\{\mathrm{b,m}\}} S & \text{for } S \geq 0 \\ r_{\{\mathrm{b,m}\}} S & \text{for } S < 0 \end{cases} \tag{18}$$

with different constant rates for synthesis (s_{b} and $s_{\mathrm{m}} = 0$) and for resorption (r_{b} and r_{m}). Of course, we remark that the synthesis of bio-resorbable material is not allowed, i.e., $s_{\mathrm{m}} = 0$. The weight function H is characterized by a U-like shape with a maximum in the neighborhood of $\phi = 0.5$ to emphasize the most effective conditions in the remodeling process. In the definition of the stimulus, the presence of a lazy zone, bounded by two thresholds ($P^{\mathrm{s}}_{\mathrm{ref}}$ and $P^{\mathrm{r}}_{\mathrm{ref}}$ for synthesis and for resorption, respectively), is hypothesized where the osteoregulatory balance of the bone is maintained. Mathematically:

$$S(\boldsymbol{X}, t) = \begin{cases} P(\boldsymbol{X}, t) - P^{\mathrm{s}}_{\mathrm{ref}} & \text{for } P(\boldsymbol{X}, t) > P^{\mathrm{s}}_{\mathrm{ref}} \\ 0 & \text{for } P^{\mathrm{r}}_{\mathrm{ref}} \leqslant P(\boldsymbol{X}, t) \leqslant P^{\mathrm{s}}_{\mathrm{ref}} \\ P(\boldsymbol{X}, t) - P^{\mathrm{r}}_{\mathrm{ref}} & \text{for } P(\boldsymbol{X}, t) < P^{\mathrm{r}}_{\mathrm{ref}} \end{cases} \tag{19}$$

The signal P related to the sensing biological activity is assumed to take the following form [26]:

$$P\,(\boldsymbol{X}, t) = \frac{\int_{\mathcal{B}} \left(\alpha\, \mathscr{E}_s + \mathscr{D}_s\right) \varpi\,(\rho^*_{\mathrm{b}})\; e^{-\frac{\|\boldsymbol{X} - \boldsymbol{X}_0\|^2}{2D^2}}\, \mathrm{d}\boldsymbol{X}_0}{\int_{\mathcal{B}} e^{-\frac{\|\boldsymbol{X} - \boldsymbol{X}_0\|^2}{2D^2}}\, \mathrm{d}\boldsymbol{X}_0} \tag{20}$$

characterized by a reference length D which delimits the range of action of the biological processes. $\mathscr{E}_s$ is the density of strain energy of the solid matrix (including first and second gradient terms) and $\varpi = 0.2\rho^*_{\mathrm{b}}/\hat{\rho}_{\mathrm{b}}$ is the density of active sensor cells assumed to be present only in the living bone tissue.

4. Numerical results

In order to show that the model presented is able to describe some possible mechanisms of bone remodeling among those induced by the presence of bio-material, the simple case outlined in Sec. 2 is numerically analyzed. For this purpose, an iterative procedure is implemented as sketch below. At first, the apparent mass density fields, for both bone tissue and bio-material, are evaluated starting from the given initial values and at any subsequent time step; subsequently, at each time step the mechanical equilibrium Eq. (14) is solved with a FE method (using COMSOL Multiphysics) under the specific boundary conditions considered; then, using the results of the two previous steps, the stimulus distribution in the body is computed with Eq. (20); finally, by means of the remodeling evolution Eq. (17), the rate of the apparent mass densities is determined and so the procedure goes back to the first step. Specifically, to overcome the limitation of a finite element code (COMSOL Multiphysics) optimized for constitutive models of the first gradient continua, it was decided to find a micromorphic model of the first gradient that was equivalent to the second gradient model, using the technique of Lagrange multipliers [40]. A further improvement can be achieved employing the recent developed tools of the isogeometric analysis particularly suitable for their inherent high continuity to treat the second gradient models (see for more details e.g. [41, 42, 43, 44]). Starting from an initial apparent mass density uniform for the bone tissue ($\rho^*_{\mathrm{b}} = 0.5\hat{\rho}_{\mathrm{b}}$) and the biomaterial ($\rho^*_{\mathrm{m}} = 0.5\hat{\rho}_{\mathrm{m}}$), we perform a parametric analysis by varying the characteristic length ℓ of the second gradient governed by Eq. (9).

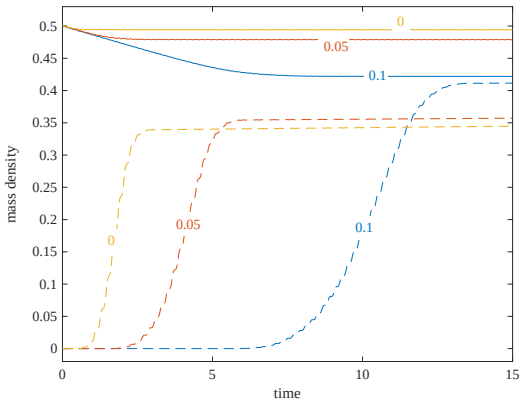

Figure 2: Time evolution of the mass densities of bone (dashed line) and material (solid line) in the probe point P_m when characteristic length ℓ is varying ($\ell = \{0, 0.05L, 0.1L\}$).

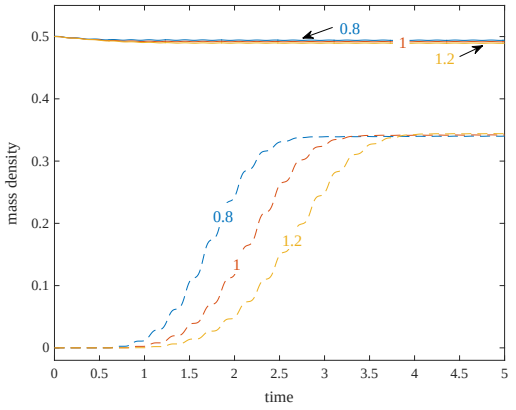

Figure 3: Time evolution of the mass densities of bone (dashed line) and material (solid line) in the probe point P_m when Y_m is varying ($Y^{\mathrm{Max}}_{\mathrm{m}} = \{0.8Y^{\mathrm{Max}}_{\mathrm{b}}, 1Y^{\mathrm{Max}}_{\mathrm{b}}, 1.2Y^{\mathrm{Max}}_{\mathrm{b}}\}$) and $\ell = 0$.

The material parameters used in the simulations are: the maximum Young modulus of the bone $Y_{\rm b}^{\rm Max} = 17$ GPa and of the bio-material $Y_{\rm m}^{\rm Max} = 0.8\, Y_{\rm b}^{\rm Max}$, the Poisson ratio $\nu = 0.3$, the real density of the bone and bio-material $\hat{\rho}_{\rm b} = \hat{\rho}_{\rm m} = 1800$ kg/m^3, the stiffness of the marrow $K_{\rm f} = 0.1\, Y_{\rm b}^{\rm Max}$, the radius of the range of action of the biological processes $D = 0.1L$, the porous non-local stiffness $K_2 = 1.7\times10^5$ N, the interface stiffnesses for porosity, displacement and gradient of displacement, $K_\zeta = 1.7\times10^7$ N/m, $K_u = 1.7 \times 10^{18}$ N/m^3 and $K_{\nabla u} = 1.7 \times 10^7$ N/m respectively, the shear viscosity $\mu^v = 2.57 \times 10^{12}$ N s/m^2, the bulk viscosity $\kappa^v = 2.06 \times 10^{12}$ N s/m^2, the rates for synthesis and for resorption $s_{\rm b} = 1.27 \times 10^{-7}$ s/m^2, $r_{\rm b} = 1.06 \times 10^{-7}$ s/m^2 and $r_{\rm m} = 1.59 \times 10^{-7}$ s/m^2, the reference thresholds for stimulus $P^{\rm s}_{\rm ref} = 1.43$ N/m^2 and $P^{\rm r}_{\rm ref} = 1.29$ N/m^2, the stimulus coefficients $\mathscr{a}$ =1, $\mathscr{b}$ = 6.048×10^6 s. The parameter defining the external load are: $F_0 = 2.0\times10^{-3}\, Y_{\rm b}^{\rm Max}$, $F_1 = F_0/2$ and $\Omega = 8.27\times10^{-7}$ Hz.

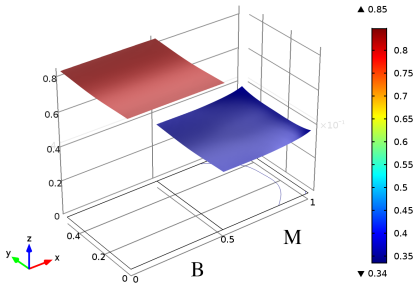

(a)

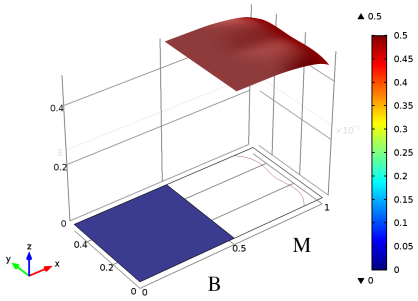

(b)

Figure 4: Distributions of the mass densities of (a) bone and (b) material at the end of the process with $\ell = 0$.

In all the following figures we plot mass densities normalized with respect to the maximum values. In Fig. 2, we compare the model of the first gradient ($\ell = 0L$) with that of the second gradient, for two different values of the characteristic length ($\ell = \{0.05L, 0.1L\}$), as reported close to the respective curves in figure. Here and henceforth, the time is normalized for the reference value of 6.048×10^5 s which corresponds about one week, lengths are normalized by L. The three dashed curves refer to the bone, while the three continuous curves relate to the material.

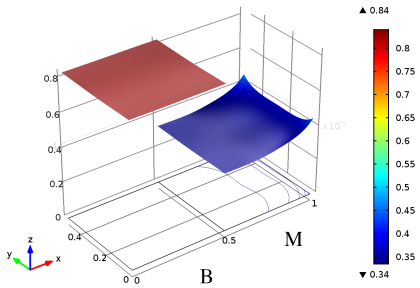

(a)

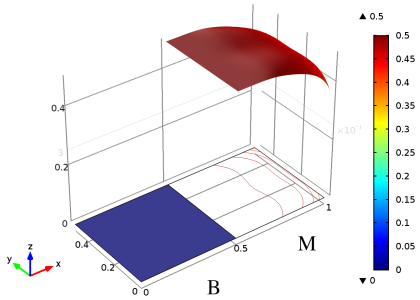

(b)

Figure 5: Distributions of the mass densities of (a) bone and (b) material at the end of the process with $\ell = 0.05\, L$.

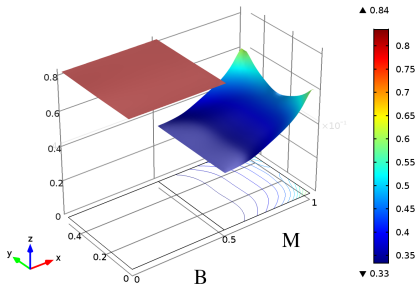

(a)

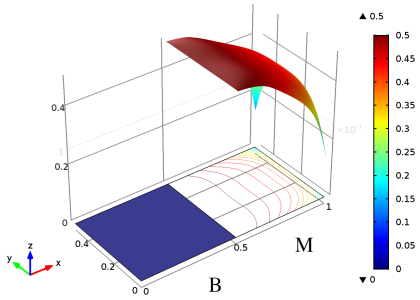

(b)

Figure 6: Distributions of the mass densities of (a) bone and (b) material at the end of the process with $\ell = 0.1\, L$.

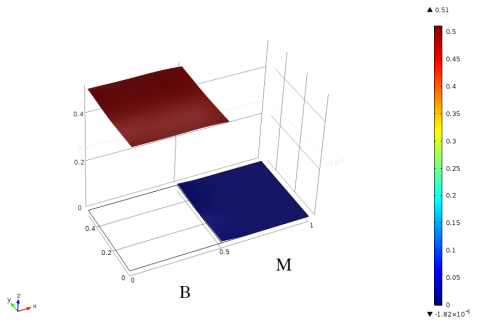

(a)

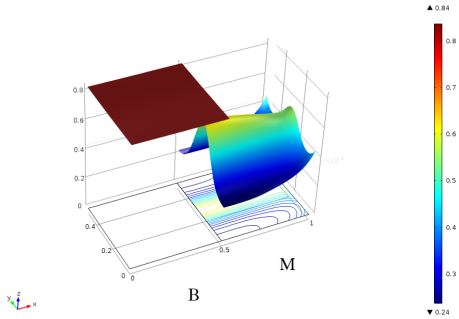

(b)

Figure 7: Distributions of bone mass density at the (a) beginning and (b) end of the process.

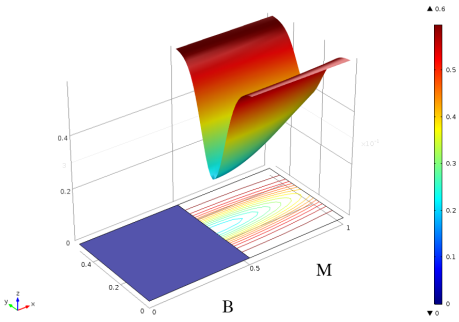

(a)

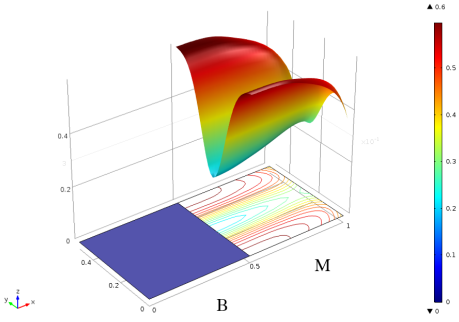

(b)

Figure 8: Distributions of material mass density at the (a) beginning and (b) end of the process.

It is observed that as the characteristic length increases, the evolutionary process takes place in a longer time and therefore the material undergoes a greater resorption and this entails that the bone has available a greater space to grow. Therefore, in the stationary state, the bone attains a greater mass density (and the material a lesser one) as the characteristic length increases. We note that this behavior is similar to that found in the case of the first gradient (Fig. 3), when increasing values of the maximum Young modulus $Y_{\mathrm{m}}^{\mathrm{Max}}$ of the bio-material are assumed. In this case, the increased stiffening, ascribable to the second gradient of displacement introduced in the constitutive relation of the mixture, is due to bending deformation at the level of microstructure. Therefore, neglecting this effect means disregarding an important contribution to the deformation energy, as seen from the simulations, which plays a significant role in the remodeling process. Figure 4 shows the situation at the end of the adaptation process in terms of apparent mass density of bone (Fig. 4a) and biomaterial (Fig. 4b), when the model of the first gradient is used. Here and henceforth, the labels "B" and "M" stand for bone and graft material, respectively. Figure 4 serves as a reference to compare the results found via the second gradient model, respectively with characteristic lengths $0.05L$ (Fig.5) and $0.1L$ (Fig.6). Figures 5 and 6 show the distributions of the apparent mass density of (a) bone and (b) biomaterial at the end of the process with the second gradient model with $\ell = 0.05L$ (Fig. 5) and $\ell = 0.1L$ (Fig. 6). It can be observed that the main differences are located in the area in the vicinity of the application of load (see Fig. 1) and further from the bone area. The portions of resorbed biomaterial and deposited bone grow with increasing characteristic length. To facilitate the understanding of the distribution of mass density in Figs. 4, 5, and 6, the level curves in plan have been reported too. In order to design the mass density to optimize the distribution of the material, it is thought to reduce the initial mass density in the neighborhood of the neutral axis (see Fig. 8a), given that the load condition is of bending. Thus, the initial (a) and final (b) states of the remodeling process, both as regards the bone (Fig. 7) and the biomaterial (Fig. 8), were compared in the case in which the initial mass density of the biomaterial is not uniform and the characteristic length is $0.07L$. In the present case the neutral axis is aligned in the longitudinal direction of the sample. It is noted that the biomaterial area with greater porosity constitutes a fast track to the bone penetrating inside the area of the material, which in fact is more dense in the area where the initial density of the biomaterial is lower, having a greater available space.

5. Conclusions

This paper presents a constitutive model for the bone-biomaterial mixture, characterized by taking into account a second gradient model. The aim was to compare the

results obtained via a simpler model of the first gradient, noting that the effect of the second gradient is to delay the process of evolution, in a manner similar to what happens when the biomaterial is stiffened under the assumption of first gradient model. This difference can be significant and therefore, it is not possible a priori ignore the effects of a second gradient without capturing this evolutionary aspect. The proposed model is characterized by several material parameters. The need to introduce these parameters is intrinsically linked to the complexity of the analyzed system. Depending on the specific cases analyzed some simplifications are possible, for instance considering the limit cases in which these parameters approach zero or infinity. However, the aim of this paper is to develop a general and flexible model which can be used in many cases significant for the study of bone reconstruction. It is clear that with a micro model very detailed, fewer parameters are required, but it is equally clear that in this case a study on a sample with size suitable for applications is very expensive from a computational point of view. Thus, the use of generalized continua can improve the computational cost without losing too much predictive power at the expense of the introduction of further constitutive parameters. On the other hand, the mechanical system the authors want to study is rather complex: it would be naive to believe that it can be described with a simple model. In any case, it is impossible to do so.

This study was done assuming uniform initial mass densities of bone and biomaterial in their respective areas. It is then analyzed the case in which the mass density of the biomaterial is not uniform at the beginning of the process, resulting in a greater bone growth where the rarefaction of the biomaterial allows it.

References

[1] R. Lakes, On the torsional properties of single osteons, J. Biomech. 28 (11) (1995) 1409–1410. doi:10.1016/0021-9290(95)00057-0.

[2] P. Frasca, R. Harper, J. L. Katz, Strain and frequency dependence of shear storage modulus for human single osteons and cortical bone microsamples—size and hydration effects, J. Biomech. 14 (10) (1981) 679–690. doi:10.1016/0021-9290(81)90050-6.

[3] J. F. C. Yang, R. S. Lakes, Transient study of couple stress effects in compact bone: torsion, J Biomech Eng. 103 (4) (1981) 275–279. doi:10.1115/1.3138292.

[4] J. F. C. Yang, R. S. Lakes, Experimental study of micropolar and couple stress elasticity in compact bone in bending, J. Biomech. 15 (2) (1982) 91–98. doi:10.1016/0021-9290(82)90040-9.

[5] H. C. Park, R. S. Lakes, Cosserat micromechanics of human bone: strain redistribution by a hydration sensitive constituent, J. Biomech. 19 (5) (1986) 385–397. doi:10.1016/0021-9290(86)90015-1.

[6] P. M. Buechner, R. S. Lakes, Size effects in the elasticity and viscoelasticity of bone, Biomech. Model. Mechanobiol. 1 (4) (2003) 295–301. doi:10.1007/s10237-002-0026-8.

[7] T. P. Harrigan, M. Jasty, R. W. Mann, W. H. Harris, Limitations of the continuum assumption in cancellous bone, J. Biomech. 21 (4) (1988) 269–275. doi:10.1016/0021-9290(88)90257-6.

[8] H. Ramézani, A. El-Hraiech, J. Jeong, C.-L. Benhamou, Size effect method application for modeling of human cancellous bone using geometrically exact cosserat elasticity, Comput. Methods Appl. Mech. Engrg. 237 (2012) 227–243. doi:10.1016/j.cma.2012.05.002.

[9] J. Fatemi, F. Van Keulen, P. R. Onck, Generalized continuum theories: Application to stress analysis in bone, Meccanica 37 (4-5) (2002) 385–396. doi:10.1023/A:1020839805384.

[10] E. Kröner, Elasticity theory of materials with long range cohesive forces, Int. J. Solids Struct. 3 (5) (1967) 731–742. doi:10.1016/0020-7683(67)90049-2.

[11] A. C. Eringen, D. G. B. Edelen, On nonlocal elasticity, Int. J. Eng. Sci. 10 (3) (1972) 233–248. doi:10.1016/0020-7225(72)90039-0.

[12] A. Madeo, D. George, T. Lekszycki, M. Nierenberger, Y. Rémond, A second gradient continuum model accounting for some effects of micro-structure on reconstructed bone remodelling, C R Mecanique 340 (8) (2012) 575–589. doi:10.1016/j.crme.2012.05.003.

[13] F. dell'Isola, P. Seppecher, A. Della Corte, The postulations á la D'Alembert and á la Cauchy for higher gradient continuum theories are equivalent: a review of existing results, Proc. R. Soc. A 471 (2183) (2015) 20150415. doi:10.1098/rspa.2015.0415.

[14] J.-J. Alibert, A. Della Corte, Second-gradient continua as homogenized limit of pantographic microstructured plates: a rigorous proof, Z. Angew. Math. Phys. 66 (5) (2015) 2855–2870. doi:10.1007/s00033-015-0526-x.

[15] E. Cosserat, F. Cosserat, Théorie des corps déformables, Librairie Scientifique A. Hermann et Fils, Paris, 1909.

[16] H. Altenbach, V. A. Eremeyev, On the linear theory of micropolar plates, Z. Angew. Math. Mech 89 (4) (2009) 242–256. doi:10.1002/zamm.200800207.

[17] J. Altenbach, H. Altenbach, V. A. Eremeyev, On generalized Cosserat-type theories of plates and shells: a short review and bibliography, Arch. Appl. Mech. 80 (1) (2010) 73–92. doi:10.1007/s00419-009-0365-3.

[18] J. L. Bleustein, A note on the boundary conditions of Toupin's strain-gradient theory, Int. J. Solids Struct. 3 (6) (1967) 1053–1057. doi:10.1016/0020-7683(67)90029-7.

[19] R. D. Mindlin, Micro-structure in linear elasticity, Arch. Rational Mech. Anal. 16 (1) (1964) 51–78. doi:10.1007/BF00248490.

[20] R. A. Toupin, Elastic materials with couple-stresses, Arch. Rational Mech. Anal. 11 (1) (1962) 385–414. doi:10.1007/BF00253945.

[21] T. San Antonio, M. Ciaccia, C. Müller-Karger, E. Casanova, Orientation of orthotropic material properties in a femur FE model: A method based on the principal stresses directions, Med. Eng. Phys. 34 (7) (2012) 914–919. doi:10.1016/j.medengphy.2011.10.008.

[22] W. C. H. Parr, U. Chamoli, A. Jones, W. R. Walsh, S. Wroe, Finite element micro-modelling of a human ankle bone reveals the importance of the trabecular network to mechanical performance: New methods for the generation and comparison of 3D models, J. Biomech. 46 (1) (2013) 200–205. doi:10.1016/j.jbiomech.2012.11.011.

[23] C. Pideri, P. Seppecher, A second gradient material resulting from the homogenization of an heterogeneous linear elastic medium, Continuum Mech. Therm. 9 (1997) 241–257. doi:10.1007/s001610050069.

[24] D. J. Steigmann, F. dell'Isola, Mechanical response of fabric sheets to three-dimensional bending, twisting, and stretching, Acta Mech. Sin. 31 (3) (2015) 373–382. doi:10.1007/s10409-015-0413-x.

[25] U. Andreaus, F. dell'Isola, I. Giorgio, L. Placidi, T. Lekszycki, N. L. Rizzi, Numerical simulations of classical problems in two-dimensional (non) linear second gradient elasticity, Int. J. Eng. Sci. 108 (2016) 34–50. doi:10.1016/j.ijengsci.2016.08.003.

[26] I. Giorgio, U. Andreaus, D. Scerrato, F. dell'Isola, A visco-poroelastic model of functional adaptation in bones reconstructed with bio-resorbable materials, Biomech. Model. Mechanobiol. 15 (5) (2016) 1325–1343. doi:10.1007/s10237-016-0765-6.

[27] M. A. Biot, Mechanics of deformation and acoustic propagation in porous media, J. Appl. Phys. 33 (4) (1962) 1482–1498. doi:10.1063/1.1728759.

[28] S. C. Cowin, Bone poroelasticity, J. Biomech. 32 (3) (1999) 217–238. doi:10.1016/S0021-9290(98)00161-4.

[29] L. Placidi, U. Andreaus, A. Della Corte, T. Lekszycki, Gedanken experiments for the determination of two-dimensional linear second gradient elasticity coefficients, Z. Angew. Math. Phys. 66 (6) (2015) 3699–3725. doi:10.1007/s00033-015-0588-9.

[30] F. dell'Isola, G. Sciarra, S. Vidoli, Generalized Hooke's law for isotropic second gradient materials, Proc. R. Soc. A 465 (2009) 2177–2196. doi:10.1098/rspa.2008.0530.

[31] A. E. Green, R. S. Rivlin, Multipolar continuum mechanics, Arch. Rational Mech. Anal. 17 (1964) 113–147. doi:10.1007/BF00253051.

[32] C. Polizzotto, A note on the higher order strain and stress tensors within deformation gradient elasticity theories: Physical interpretations and comparisons, Int. J. Solids Struct. 90 (2016) 116–121. doi:10.1016/j.ijsolstr.2016.04.001.

[33] I. Goda, M. Assidi, S. Belouettar, J. F. Ganghoffer, A micropolar anisotropic constitutive model of cancellous bone from discrete homogenization, J Mech Behav Biomed Mater 16 (2012) 87–108. doi:10.1016/j.jmbbm.2012.07.012.

[34] A. Cecchi, N. L. Rizzi, Heterogeneous elastic solids: A mixed homogenization-rigidification technique, Int. J. Solids Struct. 38 (1) (2001) 29–36. doi:10.1016/S0020-7683(00)00018-4.

[35] L. Placidi, A variational approach for a nonlinear 1-dimensional second gradient continuum damage model, Continuum Mech Therm 27 (4-5) (2015) 623–638. doi:10.1007/s00161-014-0338-9.

[36] L. Placidi, A variational approach for a nonlinear one-dimensional damage-elasto-plastic second-gradient continuum model, Continuum Mech Therm 28 (1-2) (2016) 119–137. doi:10.1007/s00161-014-0405-2.

[37] A. Misra, V. Singh, Micromechanical model for viscoelastic materials undergoing damage, Continuum Mech Therm 25 (2-4) (2013) 343–358. doi:10.1007/s00161-012-0262-9.

[38] T. Lekszycki, F. dell'Isola, A mixture model with evolving mass densities for describing synthesis and resorption phenomena in bones reconstructed with bio-resorbable materials, Z. Angew. Math. Mech 92 (6) (2012) 426–444. doi:10.1002/zamm.201100082.

[39] U. Andreaus, I. Giorgio, A. Madeo, Modeling of the interaction between bone tissue and resorbable biomaterial as linear elastic materials with voids, Z.

Angew. Math. Phys. 66 (1) (2015) 209–237. doi:10.1007/s00033-014-0403-z.

[40] S. Forest, Micromorphic approach for gradient elasticity, viscoplasticity, and damage, J. Eng. Mech. 135 (3) (2009) 117–131. doi:10.1061/(ASCE)0733-9399(2009)135:3(117).

[41] A. Cazzani, M. Malagù, E. Turco, Isogeometric analysis of plane-curved beams, Math. Mech. Solids 21 (5) (2016) 562–577. doi:10.1177/1081286514531265.

[42] A. Cazzani, M. Malagù, E. Turco, F. Stochino, Constitutive models for strongly curved beams in the frame of isogeometric analysis, Math. Mech. Solids 21 (2016) 183–209. doi:10.1177/1081286515577043.

[43] L. Greco, M. Cuomo, An isogeometric implicit G1 mixed finite element for Kirchhoff space rods, Comput Methods Appl Mech Eng 298 (2016) 325–349. doi:10.1016/j.cma.2015.06.014.

[44] L. Greco, M. Cuomo, An implicit G1 multi patch B-spline interpolation for Kirchhoff–Love space rod, Comput Methods Appl Mech Eng 269 (2014) 173–197. doi:10.1016/j.cma.2013.09.018.